Model identification and reduction for the control of an ice cream crystallization process

Céline Casenave, Denis Dochain, Graciela Alvarez, Marcela Arellano, Hayat Benkhelifa, Denis Leducq

Model identification and reduction for the control of an ice cream crystallization process[☆]

Céline Casenave[☆☆,a,b], Denis Dochain[c], Graciela Alvarez[d], Marcela Arellano[e], Hayat Benkhelifa[f], Denis Leducq[d]

[a]*UMR INRA-SupAgro 0729 MISTEA, 2 place Viala 34060 Montpellier France*
[b]*MODEMIC project-team, INRA/INRIA, Sophia-Antipolis, France*
[c]*ICTEAM, UCL, 4 avenue Georges Lemaître 1348 Louvain-la-neuve, Belgium (e-mail: denis.dochain@uclouvain.be)*
[d]*IRSTEA, 1 rue Pierre-Gilles de Gennes, 92160 Antony, France (e-mail: {graciela.alvarez, denis.leducq}@irstea.fr)*
[e]*School of Chemical Engineering, University of Birmingham, Edgbaston, Birmingham, B15 2TT, United Kingdom.*
[f]*AgroParisTech , UMR n°1145 Ingénierie-Procédés-Aliments, 16 rue Claude Bernard, 75231 Paris Cedex 05, France. (e-mail: hayat.benkhelifa@agroparistech.fr)*

Abstract

Ice cream crystallization processes can be modeled by some population and energy balance equations. Due to the infinite dimensional and nonlinear characteristics, such models are highly complex, especially when all the phenomena of nucleation, growth and breakage are considered. Depending on the control problem under consideration, such a complexity can be useless and the control law can be designed on the basis of an input-output reduced order model of the process. In the present paper, we first consider a reduced order model of 6 ordinary differential equations obtained by the method of moments. By means of a sensitivity analysis and a parameter identification, it is shown that, to accurately describe the input-output behavior of the system whatever the conditions are, it is sufficient to change the values of only two parameters of this model, which is really interesting from a control point of view. However, when looking at the simulated data, the complexity of this moments model appears useless, from the input-output point of view. A second model reduction is therefore performed, based on physical assumptions. We finally get a new model with 3 ordinary differential equations, which is validated first on experimental data and then by comparison with the initial moments model.

Keywords: ice cream crystallization, particulate processes, population balance equation, model identification, model reduction, process control

1. Introduction

Crystallization (e.g. Mullin (2001)) is encountered in many processes, in particular in the pharmaceutical industry and the food industry (Hartel, 2001). In crystallization processes, an important challenge is to control the quality and/or the properties of the product. In the case of ice creams, it is well known that the quality, that is the hardness and the texture of the ice cream, depends on the ice crystal size distribution (CSD). For example, depending on the mean crystal size, or more precisely on the dispersion of crystal sizes (that is on the shape of the CSD), the obtained texture of the ice cream is more or less grainy. Some physical properties of the ice cream, as for example its viscosity, also depend on the CSD, or at least on its moments.

In the model considered in this paper, the evolution of the CSD is described by a population balance equation (PBE) (Randolph, 1971; Costa et al., 2007) to which an energy balance equation is added. Due to the infinite dimensional and nonlinear characteristics, the model is highly complex, especially when all the phenomena of nucleation, growth and breakage (Cook and Hartel, 2010) are considered. To control such a system, and more generally the particulate processes, there exists several approaches (see for example Christofides et al. (2008) and Nagy et al. (2008)). In some papers, the proposed control law is designed directly from the PBE (Mesbah et al., 2012; Sheikhzadeh et al., 2008). It enables to take into account the whole complexity of the system dynamics but in return, it often needs sophisticated mathematical tools and can lead to some complex controllers, not always easy to implement. That's why most of the time, a reduced order model (*early lumping* - see Ray (1978)) is considered. Some examples of model reduction techniques for particulate processes can be found in Christofides (2002), Dokucu et al. (2008) or Motz et al. (2004). One of these techniques consists in applying the method of moments (Christofides, 2002), which transforms the PBE in an infinite set of moments equations (ordinary differential equations - ODEs). The number of moments equations we will finally keep, and the closure of the truncated system are some important questions. In our case, the first four moment equations are independent of the higher order ones, and the energy balance equation only involves moments of order 3 or less, so that the system we consider is finally reduced to a set of 5 ODEs. Note that this model is not well adapted for all control problems. In particular, the control of the shape of the CSD, which is of importance in crystallization processes (Vollmer and Raisch,

[☆]This work was supported by the 7th Framework Program of the European Union: CAFE Project (Computer-Aided Food processes for control Engineering project) - Large Collaborative Project KBBE-2007-2-3-01.

[☆☆]Corresponding author at: MODEMIC project-team (INRA/INRIA), UMR INRA-SupAgro 0729 MISTEA, 2 place Viala 34060 Montpellier France. Tel.: +33 4 99 61 26 96. E-mail address: celine.casenave@supagro.inra.fr (C. Casenave).

2006; Nagy, 2008; Ma and Wang, 2012), is not the kind of problems we will focus on. Indeed, it is well known that the reconstruction of a distribution from its moments is really difficult. However, the control of all quantities which can be expressed as a function of the 4 first moments and of the ice temperature (Mantzaris and Daoutidis, 2004) can be performed on the basis of this reduced order moments model.

The first part of the paper deals with the identification of the model parameters and the validation of this model by comparison with experimental data. A sensitivity analysis is performed in order to determine the parameters to be identified. To complete the model of 5 ODEs, an additive equation, which describes the dynamics of the compressor of the crystallizer is proposed and identified from experimental data.

One objective of the present paper is also to propose (and identify) a model suitable for control purposes, that is, which appropriately describes the dynamic input-output behavior of the system. In our case, we are interested in the dynamical response of the saturation temperature[1] to the variations of the refrigerant fluid temperature. To approximate such a dynamic behavior, some of the state variables of the model appear to be useless (when looking at the simulated data). Based on physical assumptions, a second model reduction is therefore proposed which finally leads to a new model only composed of 3 ODEs.

The paper is organized as follows. The experimental setup and the model of the crystallizer are described in sections 2 and 3. The identification of the moments model from experimental data is then presented in section 4. To complete the modeling, a model of the compressor is proposed and identified in section 5. Some examples of simulated trajectories are finally compared with experimental data in section 6. In section 7 the second model reduction is presented. Finally a comparison between the moments model and the reduced order one is performed in section 8.

2. Process description

2.1. Pilot plant

The pilot plant is located at IRSTEA Antony (France). The ice cream crystallizer is a 0.40 meter long cylindric Scraped-Surface Heat Exchanger (SSHE), with inner diameter of 0.05 meter (see Figure 1). The sorbet mix, which is mainly composed of sugar, gum and water, is first put in a mix storage tank which is refrigerated at a temperature T_0 of 5°C. The sorbet mix is then fed to the crystallizer by a piston pump with a mass flow rate denoted m_{fr}. Within the vessel jacket of the crystallizer, a refrigerant fluid (R22), whose temperature T_e is called the evaporation temperature, is continually vaporizing to cool down the sorbet mix and mainly to crystallize (to freeze) water in the sorbet. When the temperature of the sorbet mix goes below the saturation temperature (denoted T_{sat}), the crystallization occurs. Some ice crystals appear on the inner wall of the cylinder (nucleation). Then, these crystals are scraped by two scraper blades which turn with a rotation speed denoted N_{scrap} and so mix the ice.

[1]The saturation temperature of the ice is a threshold temperature, below which the crystallization occurs. It can be linked to the ice cream viscosity, the control of which is interesting in a production point of view.

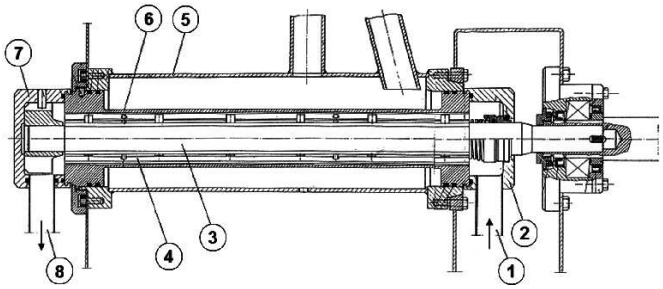

Figure 1: **Schematic representation of the SSHE (Scraped-Surface Heat Exchanger) WCB Model MF 50.** 1. Inlet connection for sorbet mix. 2. Inlet cover bowl. 3. Rotor. 4. Scraper blades rows. 5. Heat exchange cylinder jacket with vaporizing R22. 6. Heat exchange cylinder. 7. Outlet cover bowl. 8. Outlet pipe for sorbet.

The dasher rotation speed N_{scrap} and the mass flow rate m_{fr} can be varied directly by the user, which is not the case of the evaporation temperature T_e. The temperature of the refrigerant fluid is indeed modified by means of a compressor, whose rotation speed is denoted V_{comp}. The ranges of admissible values for the 3 inputs V_{comp}, N_{scrap} and m_{fr} are given in Table 1.

Inputs	Lower bound	Upper bound
Compressor rotation speed V_{comp}	500 rpm	2600 rpm
Dasher rotation speed N_{scrap}	300 rpm	1000 rpm
Mass flow rate m_{fr}	20 kg.h^{-1}	100 kg.h^{-1}

Table 1: **Bounds on the control inputs**. rpm stands for 'rotation per minute'.

2.2. Available measurements

Two variables are accessible for on-line measurement : the outlet temperature T of the ice cream and the evaporation temperature T_e. These quantities are measured every 5 seconds.

The temperature T is not measured directly at the outlet of the freezer, but further in the outlet pipe. At the measurement point, the temperature T can be reasonably considered to be equal to the saturation temperature T_{sat}. Indeed, inside the freezer, the temperature is lower than the saturation temperature so that the crystallization can proceed. But, when the ice leaves the reactor through a non refrigerated pipe, there is no more crystallization. The temperature of the ice increases until it reaches the saturation temperature value. The location of the measurement point at some distance of the reactor outlet also generates measurement delay. By denoting $T_{sat,m}$ the temperature measurement, we can assume that :

$$T_{sat,m}(t) = T_{sat}(t - d) \quad (1)$$

where T_{sat} is the saturation temperature of the ice at the outlet of the freezer and d is the measurement delay.

Note that the ice mean chord length (MCL) of sorbet was also measured by using the focus beam reflectance method (FBRM)

(see in Arellano et al. (2012)). As these measurements are only made at equilibrium, they are only used to validate the model reduction (see section 7.1).

Remark 1. The moments of the CSD are quantities that are often not measurable directly. They may appear to be related under some conditions to the geometrical properties of the crystal or to some physical quantities. In our study, we will see that the saturation temperature gives an indirect measurement of the third moment M_3 of the CSD, whereas the mean chord length is related to the ratio of moments $\frac{M_1}{M_0}$.

3. Model of the crystallizer

The model of the crystallizer considered in this paper is composed of one population balance equation describing the evolution of the CSD inside the freezer, and one energy balance equation. The definitions and units[2] of all the variables used in the sequel are given in Table 2.

3.1. Balance Equations

The ice cream crystallizer under consideration is a scraped surface heat exchanger which is assumed to behave as a plug flow reactor. The population balance equation considers transport, crystal growth, nucleation and breakage, the radial diffusion being assumed to be negligible. If the plug flow reactor is approximated, from an input-output point of view, by a Continuous Stirred-Tank Reactor (CSTR) with a transport delay[3] (to account for the fluid transport in the freezer), then we get the following simplified equation :

$$\frac{\partial \Psi}{\partial t} = \underbrace{-D\Psi}_{\text{transport}} - \underbrace{\frac{\partial (G\Psi)}{\partial L}}_{\text{growth}} + \underbrace{N\delta_{(L-L_c)}}_{\text{nucleation}} + \underbrace{B_b}_{\text{breakage}} \tag{2}$$

where δ denotes the Dirac function and the dilution rate D is deduced from the mass flow rate m_{fr} by the relation:

$$D = \frac{m_{fr}}{\rho_s V}. \tag{3}$$

Growth term: the growth rate is assumed to be independent of the crystal size; it is given by:

$$G = \beta(T_{sat} - T). \tag{4}$$

In this expression, the physical meaning of the saturation temperature T_{sat} is respected: it is a threshold temperature, below which (if $T < T_{sat}$) the crystallization occurs, and the crystals grow ($G > 0$). On the contrary, if $T > T_{sat}$ (in warm temperature zones), the crystals are melting and $G < 0$.

[2]The units of the variables are the S.I. Units, except for the rotation speeds N_{scrap} and V_{comp} which are expressed in revolution per second ($r.s^{-1}$) instead of radians per second.

[3]The transport delay does not appear in the Eqs. (2) and (7) because the input variables, that is the CSD and the temperature of the mix at the inlet of the freezer, are constant variables.

Variable	Definition	Unit
Ψ	number of crystals per meter (of the freezer) per cubic meter of the solution at the outlet of the freezer	m^{-4}
M_j	j^{th} order moment	m^{j-3}
t	time variable	s
r	radial position variable	m
L	crystal size variable	m
L_c	initial crystal size	m
R_i	freezer minimum diameter	m
R_e	freezer maximum diameter	m
G	growth rate of the crystals	$m.s^{-1}$
N	nucleation rate	$m^{-4}.s^{-1}$
B_b	net increase of crystals number by breakage	$m^{-4}.s^{-1}$
T_{sat}	saturation temperature	°C
T_e	evaporation temperature	°C
T	ice temperature	°C
T_0	inlet mix temperature	°C
α	surface nucleation constant	$m^{-2}.s^{-1}.K^{-2}$
β	growth constant	$m.s^{-1}.K^{-1}$
V	volume of the freezer	m^3
ϕ_i	ice fraction	-
N_{scrap}	dasher rotation speed	$r.s^{-1}$
V_{comp}	compressor rotation speed	$r.s^{-1}$
ν	breakage power coefficient	-
ϵ	breakage constant	m^{-1}
ω	mass fraction of solutes in the unfrozen phase	-
ω_0	initial mass fraction of solute (sucrose)	-
ρ_i	mass density of ice	$kg.m^{-3}$
ρ_s	mass density of solution	$kg.m^{-3}$
U	volumetric internal energy	$J.m^{-3}$
μ	viscosity	Pa.s
$\dot{\gamma}$	effective shear rate	s^{-1}
μ_{mix}	viscosity of the unfrozen phase	Pa.s
χ	viscous dissipation coefficient	-
ξ	adjustment parameter of the viscosity	-
ΔH	specific fusion latent heat	$J.kg^{-1}$
C_s	solute specific heat capacity	$J.kg^{-1}.K^{-1}$
C_w	water specific heat capacity	$J.kg^{-1}.K^{-1}$
h_e	convective heat transfer coefficient	$W.m^{-2}.K^{-1}$
S	ratio of the periphery over the surface of the section	m^{-1}
D	dilution rate	s^{-1}
U_0	inlet energy	$J.m^{-3}$
m_{fr}	inlet mass flow rate	$kg.s^{-1}$

Table 2: **Nomenclature**.

Nucleation term: The nucleation phenomenon consists in the formation of crystals whose size is here assumed to be characterized by L_c. Only heterogeneous nucleation at the freezer wall ($r = R_e$) is considered here. The nucleation rate N is expressed by:

$$N = \alpha \frac{2\pi R_e}{V} (T_{sat} - T_e)^2 > 0. \tag{5}$$

Breakage term: Because of the scraper, the crystals can also be broken. We assume that a particle of size L' is broken into two particles of the same size L. The total volume of ice is considered unchanged by the fragmentation[4] and a spherical shape is assumed (as in Arellano et al. (2013)). Under these assumptions, the relation between L' and L is given by $L' = 2^{1/3}L$ and the net increase of particles by breakage B_b, can be expressed

[4]The sum of the volume of the 2 crystals of size L equals the volume of the crystal of size L'.

as in Arellano et al. (2013) by:

$$B_{\mathrm{b}} = \epsilon N_{\mathrm{scrap}}\, \phi_{\mathrm{i}}^{\nu} \left(2\, 2^{2/3}\, L\Psi(\sqrt[3]{2}\, L) - L\Psi(L) \right). \tag{6}$$

The breakage power coefficient ν is taken to be equal to 0, as in Gonzalez et al. (2011).

Under the same hypotheses than for the population balance equation, the energy balance equation is written as follows :

$$\frac{dU}{dt} = \underbrace{D(U_0 - U)}_{\text{transport}} + \underbrace{h_{\mathrm{e}} S (T_{\mathrm{e}} - T)}_{\text{wall heat transfer}} + \underbrace{\mu \dot{\gamma}^2}_{\text{viscous dissipation}} \tag{7}$$

$$\text{with: } \dot{\gamma} = 2\pi\chi N_{\mathrm{scrap}} \text{ and } S = \frac{2R_{\mathrm{e}}}{R_{\mathrm{e}}^2 - R_{\mathrm{i}}^2}. \tag{8}$$

3.2. Moments model

Applying the method of moments[5] to equation (2), we get, for all $j \geqslant 0$ (Gonzalez et al. (2011)) :

$$\frac{dM_j}{dt} = -DM_j + jG\, M_{j-1} + N\, L_{\mathrm{c}}^j + B \left(2^{1-\frac{j}{3}} - 1 \right) M_{j+1} \tag{9}$$

where $M_j(t) = \int_0^\infty L^j \Psi(L,t) dL$ is the j^{th} order moment of the CSD, and:

$$B = \epsilon N_{\mathrm{scrap}}. \tag{10}$$

Moreover Eq. (7) can be rewritten with the temperature T as the state variable by using the following relation :

$$U = -\Delta H \rho_i \phi_i + \rho_s \left(\omega_0 C_s + (1 - \omega_0) C_w \right) T. \tag{11}$$

If we consider the ice crystals as spherical particles (as in Arellano et al. (2013)), then we have:

$$\phi_{\mathrm{i}} = \frac{\pi}{6} M_3, \tag{12}$$

which, after computations, leads to :

$$\frac{dT}{dt} = D\,(T_0 - T) + K_2\,(T_{\mathrm{e}} - T) + N_{\mathrm{scrap}}^2 K_3 \mu + K_1 \left(3GM_2 + NL_{\mathrm{c}}^3 \right) \tag{13}$$

with the following quantities :

$$K_0 = \rho_s \left(\omega_0\, C_{\mathrm{s}} + (1 - \omega_0) C_{\mathrm{w}} \right),\ T_0 = \frac{U_0}{K_0}, \tag{14}$$

$$K_1 = \frac{\pi}{6} \frac{\Delta H\, \rho_i}{K_0},\ K_2 = \frac{h_{\mathrm{e}} S}{K_0},\ K_3 = \frac{(2\pi\chi)^2}{K_0}. \tag{15}$$

The saturation temperature is supposed to depend only on M_3, that is $T_{\mathrm{sat}} = T_{\mathrm{sat}}(M_3)$. As a consequence, G and N can be expressed as functions of the variables M_3 and T, and M_3 and T_{e} respectively (i.e. $G = G(M_3, T)$ and $N = N(M_3, T_{\mathrm{e}})$). So, if the viscosity μ is assumed to depend only on the third moment M_3, the temperature T, and the dasher rotation speed N_{scrap} (i.e. $\mu = \mu(M_3, T, N_{\mathrm{scrap}})$), then the system composed of the four first moment equations and the temperature equation is closed. The closure of the system derives from the assumptions that the total volume of ice is preserved by the fragmentation, and that the crystals are spherical. Indeed, under these hypotheses, the third moment M_3 is proportional to the total volume of ice, and, as a consequence, is also preserved by the fragmentation. Concretely, these assumptions lead to the cancellation of the breakage term in the equation of M_3 ($2^{1-\frac{j}{3}} - 1 = 0$ for $j = 3$), and therefore to the closure of the equations of moments.

In the sequel we shall therefore consider the following model :

$$\frac{dM_0}{dt} = -DM_0 + N + BM_1 \tag{16}$$

$$\frac{dM_1}{dt} = -DM_1 + GM_0 + NL_{\mathrm{c}} + c_1 BM_2 \tag{17}$$

$$\frac{dM_2}{dt} = -DM_2 + 2GM_1 + NL_{\mathrm{c}}^2 + c_2 BM_3 \tag{18}$$

$$\frac{dM_3}{dt} = -DM_3 + 3GM_2 + NL_{\mathrm{c}}^3 \tag{19}$$

$$\frac{dT}{dt} = D\,(T_0 - T) + K_2\,(T_{\mathrm{e}} - T) + N_{\mathrm{scrap}}^2 K_3 \mu + K_1 \left(3GM_2 + NL_{\mathrm{c}}^3 \right) \tag{20}$$

with $\mu = \mu(M_3, T, N_{\mathrm{scrap}})$, $G = G(M_3, T)$, $N = N(M_3, T_{\mathrm{e}})$, $B = B(N_{\mathrm{scrap}})$ and the constants $c_1 = 2^{\frac{2}{3}} - 1$ and $c_2 = 2^{\frac{1}{3}} - 1$.

This model is a dynamic version of the one developed by research teams of AgroParisTech and IRSTEA Antony (France), and described in Arellano et al. (2013) and Gonzalez et al. (2011).

3.3. Characteristic quantities of the product

The saturation temperature and the viscosity of the ice both depend on the formula of the mix used (mainly on ingredients content) and on the desired final product. The sorbet considered in this study is only composed of water, gum and sugar, and no air is added during the crystallization.

Saturation temperature: The expression of the saturation temperature (in [°C]) has been determined experimentally from the commercial mix (Gonzalez, 2012); it is given by:

$$T_{\mathrm{sat}}(M_3) = -7.683\omega + 8.64\omega^2 - 70.1\omega^3, \tag{21}$$

where, the mass fraction of sugar in the unfrozen phase, ω, depends on the ice fraction ϕ_i in the following way:

$$\omega = \frac{\omega_0}{1 - \frac{\rho_i}{\rho_s}\phi_i} = \frac{\omega_0}{1 - \frac{\rho_i}{\rho_s}\frac{\pi}{6} M_3}. \tag{22}$$

According to the "liquidus curve" experimentally determined for the sorbet mix in Gonzalez (2012), T_{sat} is a decreasing function[6] of M_3.

Viscosity: the expression of the viscosity (in $[Pa.s]$) has been

[5] The method of moments consists in multiplying the population balance equation by L^j and then integrating it from $L = 0$ to $L = \infty$.

[6] The derivative of function T_{sat} is given by $T'_{\mathrm{sat}}(M_3) = \frac{\rho_i}{\rho_s} \frac{pi}{6} \frac{\omega^2}{\omega_0} \times \left(-7.683 + 2 \times 8.64\omega - 3 \times 70.1\omega^2 \right) < 0$.

obtained empirically in Gonzalez (2012); it is given by:

$$\mu(M_3, T, N_{\text{scrap}}) = \mu_{\text{mix}} \times \left(1 + 2.5\,\phi_i + 10.05\,\phi_i^2 + 0.00273\,\xi\, e^{16.6\,\phi_i}\right), \tag{23}$$

where μ_{mix}, the viscosity of the unfrozen phase, is given by:

$$\mu_{\text{mix}} = 39.02 \times 10^{-9} \times \dot{\gamma}^{0.600-1} e^{\frac{2242.38}{T+273}} \times (100\,\omega)^{2.557}. \tag{24}$$

4. Parameter identification and validation of the model of the crystallizer

The model under consideration in this paper will then be used for a control purpose. More precisely, the goal is in the end to control the saturation temperature of the ice cream at the outlet of the freezer. As the control input is the evaporation temperature, the objective of the modeling is to accurately describe the input-output behavior of the system, that is the dynamical response of the saturation temperature T_{sat} to the input T_{e}. As a consequence, the model will be validated by comparison between the simulated saturation temperature values and the measured ones. Before that, a sensitivity analysis followed by an identification step will be performed, to first determine the more sensitive parameters and then estimate their values. For a review about model identification for crystallization processes, one can refer to Rawlings et al. (1993).

4.1. Sensitivity analysis

Before identifying the parameters model, we first study the sensitivity of the model to its parameters. To evaluate the effect of the variation of a parameter on the model, we use the following quantity (as in Bernard et al. (2001)):

$$\sigma_x(p) = \frac{1}{T} \int_{t_0}^{t_0+T} \left| \frac{x(t, X_0, p) - x(t, X_0, p^{\text{ref}})}{x(t, X_0, p^{\text{ref}})} \right| dt, \tag{25}$$

where x is a variable of the model, p is the parameter, X_0 is the initial conditions of the model, t_0 is the initial time and $t_0 + T$ is the given final time, p^{ref} is the reference value of parameter p and $x(t, X_0, p)$ is the value of the variable x at time t obtained by simulation of the model with initial conditions X_0 and parameters value p. The quantity $\sigma_x(p)$ can be viewed as a mean relative difference between the reference value $x(t, X_0, p^{\text{ref}})$ of x and the one obtained for the parameter value p.

The value of $\sigma_x(p)$ has been computed for the parameters ϵ, L_{c}, α, β, h_{e}, ξ and χ, which, among all the parameters of the model, are the ones which are either ill-known or possibly dependent on some neglected phenomena or external environmental conditions (as, for example, the temperature of the room in which the freezer is located). In comparison, R_i, R_e, V are some constant physical parameters depending on the geometry of the freezer; ρ_i, ρ_s, ΔH, C_s, C_w are well-known constants; and ω_0 and T_0 respectively depend on the mix and the process.

As for the variable x, the effect on all the state variables M_0, M_1, M_2, M_3, and T and the one on T_{sat} have been studied. However, as explained before, we focus more specifically on the dynamical response of the saturation temperature.

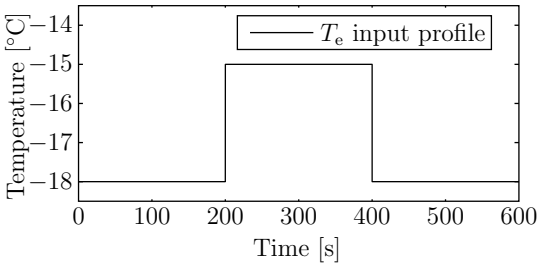

Figure 2: **Sensitivity analysis**: profile of the input T_{e} used for the computation of $\sigma_x(p)$.

T_0	5°C	L_{c}	$5\,10^{-6}$ m	ρ_i	1000 kg.m^{-3}
ν	0	R_i	0.016 m	ρ_s	1100 kg.m^{-3}
ϵ	20 m^{-1}	R_e	0.025 m	ΔH	$333.6\,10^3$J.kg^{-1}
ω_0	0.25	α	$1\,10^9$ m^{-2}.s^{-1}.K^{-2}	C_s	1676 J.kg^{-1}.K^{-1}
χ	2	β	$5\,10^{-7}$ m.s^{-1}.K^{-1}	C_w	4187 J.kg^{-1}.K^{-1}
ξ	350	V	$3.87\,10^{-4}$ m^3	h_{e}	2000 W.m^{-2}.K^{-1}

Table 3: **Sensitivity analysis**: constant parameters values used for the simulation of the reference trajectories (chosen according to Arellano et al. (2013) and Gonzalez et al. (2011)).

The choice of the reference trajectories of the model is obviously important. They have been obtained by simulation of the model with the following input variable values: $N_{\text{scrap}} = 750$ rpm and $\text{m}_{\text{fr}} = 50$ kg.h^{-1}; the initial conditions $M_0(0) = M_1(0) = M_2(0) = M_3(0) = 0$, $T(0) = T_0$ which correspond to the starting up of the process; and the constant parameter values given in Table 3. The input profile of the evaporation temperature is the one given in Figure 2. Finally, the initial and final times are respectively taken equal to $t_0 = 200$ s and $t_0 + T = 600$ s, time instants at which the process is stabilized.

The results are given in Figure 3.

Parameter	Unit	b_{min}	b_{max}
ϵ	m^{-1}	0	40
L_{c}	m	0	10^{-6}
α	m^{-2}.s^{-1}.K^{-2}	3×10^8	7×10^9
β	m.s^{-1}.K^{-1}	0	7×10^{-6}
h_e	W.m^{-2}.K^{-1}	1000	4000
ξ	–	0	700
χ	–	0	40

Table 4: **Sensitivity analysis**: minimum and maximum bounds b_{min} and b_{max} of the parameters on which the sensibility analysis has been performed.

First note that the variations of ϵ, L_{c}, α and ξ have a very low impact on T_{sat}. The parameter ϵ is the breakage constant; as we assume that the volume of the ice is conserved when a crystal is divided by breakage, it can be expected that M_3 (and so T_{sat}) that represents the volume of crystals per cubic meter, is not very much affected by a variation of ϵ. The possible values of L_{c} are very small: the effect of the considered variations of L_{c} still remains too small to affect the value of M_3. This obviously makes sense, because L_{c} is linked to the nucleation phenomenon, by which the number of crystals, and not the volume, increases. For the same reason, the effect of the variation of the surface nucleation constant α is also small. Finally ξ is related to the viscosity term of the model, which, for the considered range of parameter variation, does not influence the volume of

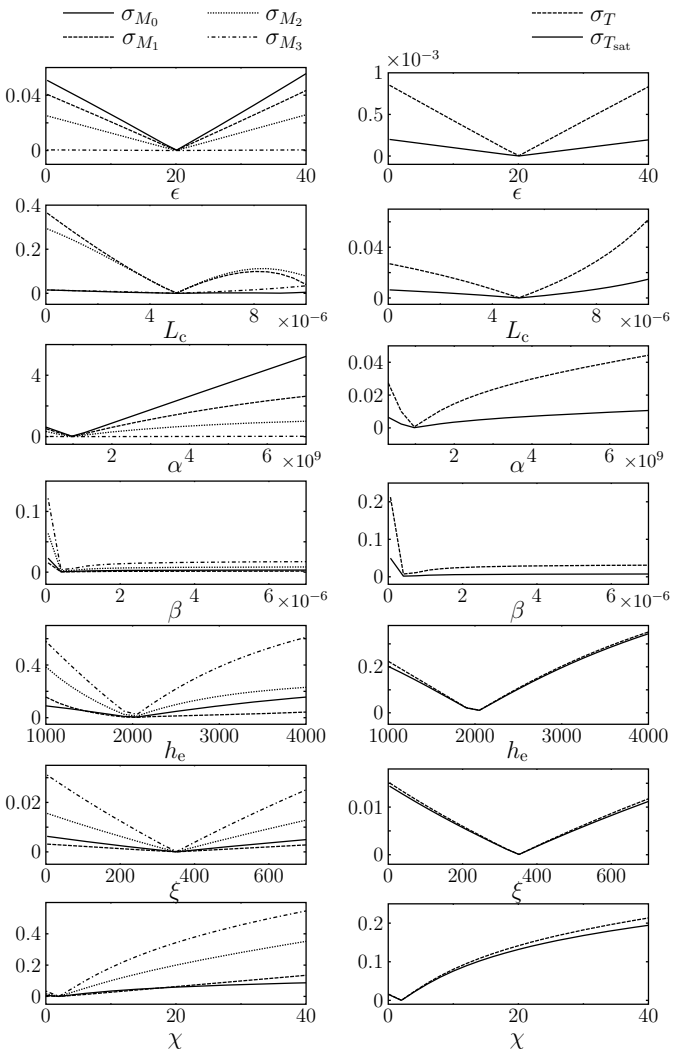

Figure 3: **Sensitivity analysis**: evolution of the quantity $\sigma_x(p)$ defined by (25) for different parameters and variables of the model, for p going from $b_{\min}$ to $b_{\max}$ (see Table 4).

the crystals a lot.

The growth constant β influences the value of T_{sat} more than the preceding parameters. This is physically consistent with the fact that the volume of the ice depends on the growth rate G. But the parameters which at the most affect T_{sat} are h_{e} end χ. It is not surprising as h_{e} is the convective heat transfer coefficient, which consequently has a direct impact on both temperatures T and T_{sat}, and χ is the viscous dissipation coefficient on which depends the temperature of the ice.

4.2. Identification of the parameters

According to the sensitivity analysis performed in Section 4.1, the saturation temperature T_{sat} is mostly influenced by the parameters h_{e} and χ. Let's now see if the identification of these two parameters is sufficient to obtain simulated trajectories close to the experimental data.

For that, we have performed several identifications from 12 sets of experimental data. The identifications were made on each of the 12 experimental data sets separately. Indeed, as it will be discussed later, some parameters of the model depend on some neglected phenomena or external environmental conditions and can therefore vary from one experiment to the other. As a consequence, it is impossible to find a unique set of parameter values for which the model will explain well the 12 experimental data sets together.

For each $i = 1 : 12$, that is for each experimental data set, we will denote in the sequel N^i the number of measurement instants, $t^{k,i}$, $k = 1 : N^i$ the measurement instants, $T^{k,i}_{\text{sat,m}}$ the measurement of the saturation temperature at time $t^{k,i}$, d^i the measurement delay, $X^{0,i}$ the initial conditions values, and $U^{k,i}$ the control inputs values at time $t^{k,i}$.

To identify the parameters (vector p in the sequel) of the model, we used the Nelder-Mead simplex method (function fminsearch of Matlab) to solve the least-squares minimization problem:

$$\hat{p} = \arg\min_p E^i(p) \tag{26}$$

where $E^i(p)$ is the least-squares error on the i^{th} experimental data set which is given by:

$$E^i(p) = \frac{1}{N^i}\sum_{k=1}^{N^i}\left(T_{\text{sat}}(t^{k,i} - d^i, X^{0,i}, U^{k,i}, p) - T^{k,i}_{\text{sat,m}}\right)^2, \tag{27}$$

with $T_{\text{sat}}(t^{k,i} - d^i, X^{0,i}, U^{k,i}, p)$ the value of the saturation temperature at time $t^{k,i} - d^i$ obtained by simulation of the model (16-20) with initial conditions $X^{0,i}$, control inputs values $U^{k,i}$ and parameters values p. The value of the measurement delay d^i considered for the identification is discussed in paragraph 4.4. The control inputs values $U^{k,i}$ are either known (the mass flow rate m_{fr} and the dasher rotation speed N_{scrap}) or measured (the evaporation temperature T_{e}). As for the initial conditions $X^{0,i} = \left(M_0^{i,0}, M_1^{i,0}, M_2^{i,0}, M_3^{i,0}, T^{i,0}\right)$, they are deduced from the measurements $T^{k,i}_{\text{sat,m}}$ of T_{sat} in the following way:

$$M_3^{i,0} = T_{\text{sat}}^{-1}(T^{0,i}_{\text{sat,m}}), \tag{28}$$

where T_{sat}^{-1} is the inverse of the restriction of function T_{sat} (see formula (21)) to the interval $\left[0, \frac{\rho_s}{\rho_i}\frac{6}{\pi}\right[$ of admissible physical values[7] of M_3; and:

$$\forall\, j \neq 3, M_j^{i,0} = \frac{M_3^{i,0}}{L_c^{3-j}} \text{ and } T^{i,0} = T^{0,i}_{\text{sat,m}} - 0.25. \tag{29}$$

The set of parameter values used for the initialization of the identification is the one given in Table 3.

The set of parameters to be identified has been divided in 3 subsets, depending on their influence on the saturation temperature value. We then have[8]:

[7] Indeed, the mass fraction of solutes in the unfrozen phase ω is necessarily positive. From (22), we then deduce that $M_3 < \frac{\rho_s}{\rho_i}\frac{6}{\pi}$

[8] Note that the parameter ε has not been identified, its influence on the saturation temperature being too small compared to any of the other parameters.

- subset 1: h_e and χ, the most influential parameters;
- subset 2: β whose influence on T_{sat} is lower;
- subset 3: α, ξ and L_c, the less influential parameters.

Based on these 3 subsets, we have performed different identifications, the number of identified parameters varying from 1 to 6 as explained in Table 5. In this table the distribution of the identified parameters in the 3 subsets is given, depending on the total number of identified parameters. For example, for an identification of 5 parameters, we will have: 2 parameters of the subset 1 (that is h_e and χ), 1 parameter of the subset 2 (that is β) and 2 parameters of the subset 3 (that is either α and ξ, α and L_c, or ξ and L_c). The values of the parameters which are not identified are the ones given in Table 3.

Parameters to be identified			
Total	Subset 1	Subset 2	Subset 3
1	1	–	–
2	2	–	–
3	2	1	–
4	2	1	1
5	2	1	2
6	2	1	3

Table 5: **Parameters identification of the freezer model**: Distribution of the parameters to be identified between the 3 subsets, depending on the total number of parameters to be identified.

The results are given in Table 6. The first line of the table corresponds with the reference model, that is the one characterized by the initial set of parameters given in Table 3. The identification results are then presented depending on the number of identified parameters. The quality of the identification is estimated in terms of comparison between the simulations of the identified model and the experimental data. For the identification of n parameters, we introduce the following quantities:

- m_E^n and σ_E^n: respectively the mean value and the standard deviation, on all the 12 experiments, of the minimal value of $E^i(p)$ on the set of all parameters distribution p of size n (see Table 5):

$$m_E^n = \frac{1}{12}\sum_{i=1}^{12} \min_{size(p)=n} E^i(p),$$

$$\sigma_E^n = \left(\frac{1}{12}\sum_{i=1}^{12}\left(\min_{size(p)=n} E^i(p)\right)^2 - m_E^2\right)^{1/2};$$

- p_E^n: the percentage of improvement of the identification results (in terms of m_E^n value, and with respect to the reference model) in comparison with the best identification results obtained with $m < n$ identified parameters:

$$p_E^n = 100 \times \frac{m_E^{b_n} - m_E^n}{m_E^0}, \text{ with } b_n = arg\min_{m<n} m_E^m.$$

For each identification, only 2/3 of the data set are used to compute the estimate $\hat{p}$, the last 1/3 being saved for the cross validation. In Table 6, we use the subscripts cv and t to point out when the computation of $E^i(p)$ (which appears in the expressions of m_E^n and σ_E^n) has been performed on the last 1/3 of the data set ("cross validation" data) or on the whole data set ("total" set of data).

n: number of parameters	$m_{E_{cv}}^n$ ($\times 10^{-2}$)	$m_{E_t}^n$ ($\times 10^{-2}$)	$\sigma_{E_t}^n$ ($\times 10^{-2}$)	$p_{E_t}^n$ (%)
0	95.3	95.8	60.6	–
1	9.38	8.04	5.61	90.2
2	1.88	0.988	0.604	8.10
3	1.90	1.00	0.583	$-3.35\,10^{-3}$
4	1.74	0.942	0.573	$5.15\,10^{-2}$
5	1.71	0.941	0.531	$-1.85\,10^{-2}$
6	1.96	1.04	0.613	$-1.67\,10^{-1}$

Table 6: **Parameters identification of the freezer model**: estimation of the quality of the identified model depending on the number of identified parameters.

From Table 6, we first conclude that the identification process consequently increases the quality of the model. Indeed, by identifying only 1 parameter (h_e or χ), the value of m_E^0 has been decreased of 90.2%.
The results of the identification of both parameters h_e and χ ($n = 2$) are even better, the value of m_E^2 being 8.10% smaller than m_E^1. However, the addition of 1 identified parameter or more ($n \geqslant 3$) does not improve the quality of the model any more. As expected from the sensitivity analysis, the identification of the two parameters h_e and χ is therefore sufficient to get an accurate model (see Section 6 for a comparison between some experimental data and the associated simulated trajectories).

We also note that the values of $m_{E_{cv}}^n$ are obviously greater than the ones of $m_{E_t}^n$ (about 2 times greater) but that they are even though sufficiently small for control purposes.

4.3. Comments on the identified values of parameters h_e and χ

The identification process presented in the previous section leads to the conclusion that the identification of parameters h_e and χ is sufficient to get a good input-output approximation of the dynamic behavior of the process. However, each identification has been performed on each data set separately. We therefore have obtained one set of identified parameter values per data set and per identification. Let's now make a few comments about the identified values.

First focus on the identified values of h_e and χ for a given set of data. For identifications of at least 2 parameters, the obtained identified value of h_e does not vary a lot from one identification to the other. At mean (on the 12 experiments), the standard deviation is indeed equal to $111.7\,W.m^{-2}.K^{-1}$, the mean values ranging from $1800\,W.m^{-2}.K^{-1}$ to $3600\,W.m^{-2}.K^{-1}$. The variations of the identified value of χ are slightly greater. To quantify these variations, we only consider identifications in which the parameter ξ is not identified. Indeed, both parameters ξ and χ are related to the viscous dissipation term. In the input-output point of view, their respective contributions to the variation of the output value can not be distinguished by the identification process. As a consequence, when ξ is also identified, the obtained identified values of χ can vary a lot in comparison with

other identifications. If we do not consider identifications in which ξ is identified, the mean standard deviation is equal to 0.1169, the mean values ranging from 0.01 to 1.02. The fact that the identified values of h_e and χ do not vary a lot with respect to the number of parameters to be identified shows that their contribution to the saturation temperature dynamic are essential and can not be compensated by other parameters.

Let now look at the identified values of h_e and χ obtained when only both of them are identified. In Table 7 the standard deviation and the minimal, maximal and mean values of h_e and χ computed on the set of the 12 experiments are given. As we

Parameter	Min	Max	Mean	Standard deviation
h_e [W.m^{-2}.K^{-1}]	1827	3486	2496	541.1
χ [−]	$3.116\,10^{-3}$	0.9782	0.4223	0.3326

Table 7: **Parameters identification of the freezer model**: identified values of h_e and χ when only both of them are identified. The standard deviation and the minimal, maximal and mean values are computed on the set of the 12 experiments.

can see, the identified values can vary significantly from one experiment to the other. As a consequence, is is impossible to find a unique set of parameters values for all the experiments. Several factors can explain the variations of the values of these parameters. For example, the heat losses to the ambiance have not been considered in the modeling: as a consequence, the parameter h_e should vary with the temperature of the room in which is located the freezer. The heat transfer between the evaporation temperature and the ice is also directly affected by the thickness of the ice layer which is formed on the wall (by nucleation). We know that this thickness varies depending on the dasher rotation speed, which is also not taken into account in the proposed model.

4.4. Measurement delay

The value d of the measurement delay has also been identified from the experimental data, using an identification process similar to the one described in Section 4.2. The obtained identified value is given in Figure 4 as a function of the mass flow rate. As we can see, the larger the mass flow rate, the smaller

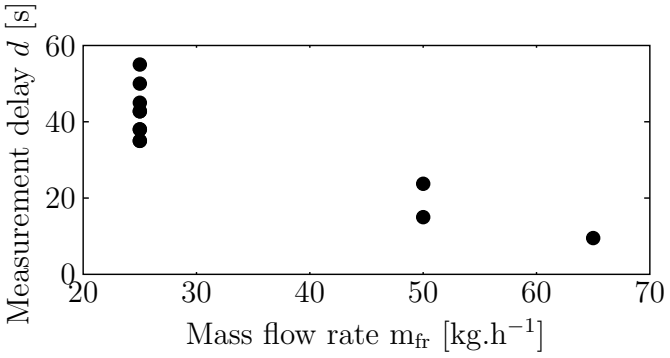

Figure 4: **Measurement delay**: identified values of the measurement delay d versus the mass flow rate m_{fr}.

the delay. Indeed, the delay measurement is mainly due to the distance between the outlet of the freezer and the measurement point: the ice reaches it more rapidly when the mass flow rate is large.

From Figure 4, we also note that, for a given value of the mass flow rate (m_{fr} = 25 kg.h^{-1} for example), the value of the measurement delay varies from one experiment to another. This can be due to several other factors, such as the viscosity of the ice, or the value of the evaporation temperature.

5. Model of the compressor

According to the responses of the evaporation temperature T_e to some step inputs of the compressor rotation speed V_{comp} (see Figure 5a.), the dynamics of the compressor (in the input V_{comp} - output T_e point of view) can be approximated by a first order equation with a nonlinear gain, i.e. :

$$\frac{dT_e}{dt} = -\frac{1}{\tau_c}T_e + \frac{1}{\tau_c}G^c, \tag{30}$$

where $G^c = G^c(V_{comp}, m_{fr})$ is the nonlinear gain which is assumed to depend on V_{comp} and m_{fr}, and τ_c is the time constant. G^c and τ_c have been identified separately.

5.1. Identification of the time constant τ_c

To identify τ_c, we used 3 experimental data sets obtained for different step inputs of the compressor rotation speed V_{comp}. The values of m_{fr}, N_{scrap}, and the initial and final values of the step input V_{comp} are given in Table 8 for each data set.

Step number	m_{fr} [kg.h^{-1}]	N_{scrap} [rpm]	Initial V_{comp} [rpm]	Final V_{comp} [rpm]
1	25	750	750	600
2	50	652	562	1025
3	65	445	1300	750

Table 8: **Identification of the model of the compressor**: values of m_{fr}, N_{crap}, and the initial and final values of the step input V_{comp} for each experimental data sets used for the identification of the time constant τ_c of the T_e dynamic.

After normalization of the data sets, we applied the Simplified Refined Instrumental Variable method for Continuous-time model (SRIVC - see Young (2002); Garnier and Young (2004)); we get the following identified value of τ_c:

$$\tau_c = 31.77\,[\text{s}]. \tag{31}$$

In Figure 5a, the trajectory obtained by simulation of model $\frac{dy}{dt} = -\frac{1}{\tau_c}y + \frac{1}{\tau_c}u(t)$ with $u(t) = -\mathbb{1}(t)$ and τ_c given by (31) is compared to the experimental normalized data; as expected, the model fits well the data.

5.2. Identification of the nonlinear gain G_c

The nonlinear gain G_c has been identified from a data set composed of 68 measurements of T_e at equilibrium, obtained for different values of m_{fr} and V_{comp}, going from 25 kg.h^{-1} to 75 kg.h^{-1} for m_{fr} and from 520 rpm to 1487 rpm for V_{comp}. As

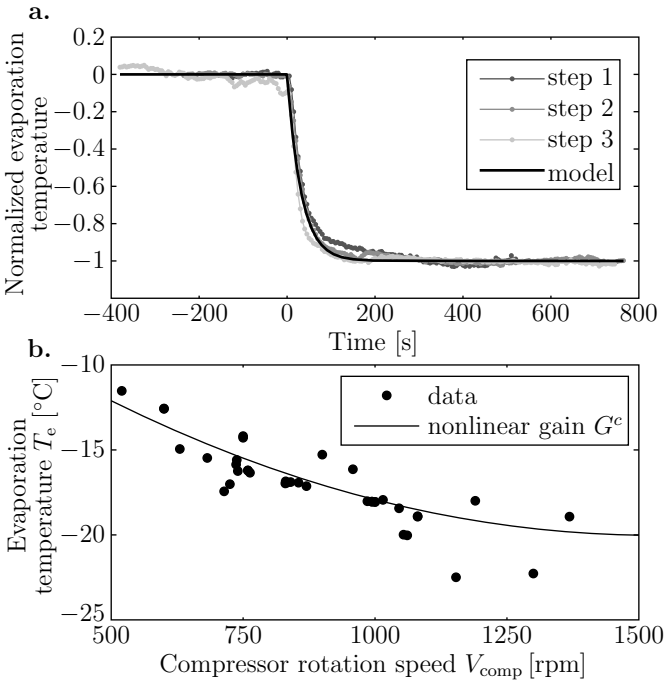

Figure 5: **Model of the compressor** a. identification of the time constant τ_c. b. identification of the nonlinear gain G_c, for $m_{fr} = 50\,kg.h^{-1}$ and $N_{scrap} = 750\,rpm$.

identification model for the nonlinear gain G_c, a polynomial function of degree 2 of the following form has been chosen:

$$f(V_{comp}, m_{fr}) = a_0 + a_1\, m_{fr} + a_2\, m_{fr}^2 + a_3\, V_{comp} + a_4\, V_{comp}^2. \quad (32)$$

The estimations of parameters $a_j,\ j = 0:4$ have been obtained by resolution of the least squares problem:

$$\left\{a_j\right\}_{j=0:4} = \arg\min_{a_j} \sum_{i=1}^{68} \left(f(V_{comp}^i, m_{fr}{}^i) - T_e^i\right)^2,$$

where $\left(V_{comp}^i, m_{fr}^i, T_e^i\right)_{i=1:68}$ are the points of the experimental data set. The obtained values of $a_j,\ j = 0:4$ are given here after:

$$a_0 = -1.122, \quad a_1 = -3.025\,10^2, \quad a_2 = 1.386\,10^4,$$
$$a_3 = -1.370, \quad a_4 = 2.687\,10^{-2}. \quad (33)$$

As an illustration, the curve of the estimated G_c as a function of V_{comp} (m_{fr} being kept constant and equal to $25\,kg.h^{-1}$) is plotted in Figure 5b. and compared to the experimental data used for the identification. As we can see, the qualitative behavior of the function is good. However, we also note that, from one experiment to the other, there can be large differences (2°C or more) between the evaporation temperature values. In the control point of view, this "modeling error" can be compensated by the control law, because it only affects the gain, and not the dynamics of T_e. But, to compare the evaporation temperature measurement data with the model (30), we have introduced in the sequel an additive adjustment parameter θ_i, which depends on the experimental data set under consideration: this parameter enables to compensate the static error. For the i^{th} experimental data set, we will therefore have :

$$G^c(V_{comp}, m_{fr}) = f(V_{comp}, m_{fr}) + \theta_i,\ \theta_i \in \mathbb{R}. \quad (34)$$

As we shall see in paragraph 6, this constant adjustment parameter will be sufficient to get a good approximation of T_e. It corresponds to a translation of the graph of function f.

6. Comparison between some simulated trajectories and experimental data

For illustration, we show in Figure 6 an example of trajectories obtained by simulation of model (16-20), after identification of parameters h_e and χ from experimental data. Their identified values are given here after:

$$h_e = 3.106\,10^3\ [W.m^{-2}.K^{-1}],\ \chi = 3.117\,10^{-3}\ [-]. \quad (35)$$

For the considered experiment (denoted experiment A in the sequel), the mass flow rate m_{fr} and the scraper rotation speed N_{scrap} were constant and respectively equal to $50\,kg.h^{-1}$ and 750 rpm. The profile of T_e is the one given in Figure 7. The simulated saturation temperature is compared to the whole set of experimental data, including the data used for the identification of h_e and χ, and the ones saved for the cross validation. We have:

$$\sum_{k=1}^{K} \left| \frac{T_{sat}^{(16-20)}(t^{k,i}) - T_{sat,m}^{k,i}}{T_{sat,m}^{k,i}} \right| \left(t^{k,i} - t^{k-1,i}\right) = 1.342\,10^{-2}, \quad (36)$$

where $T_{sat}^{(16-20)}(t^{k,i})$ is the value of the saturation temperature at time $t^{k,i}$ obtained by simulation of model (16-20).

Remark 2. The results obtained with another experimental data set (denoted experiment B in the sequel) are given in Figure 10. For this data set, the quantity defined in (36) is equal to $3.559\,10^{-3}$.

In Figure 7, the model of the compressor (30), with the identified value (31) of τ_c and the identified expression (34,33) of G_c, is compared with one experimental data set which has not been used for the identification process of τ_c and G_c (cross validation). These data correspond to the experiment A (presented in Figure 6). The adjustment parameter θ_i is taken to be equal to 0.3012 °C. It has been estimated from the first 2/3 of the data set by means of the State Variable Filter (SVF) method. As we can see, the value of T_e obtained by simulation of the model is close to the experimental data values on the whole data set (identification and cross validation parts).

7. Model reduction

As shown in the previous sections of the paper, the model (16-20) well describes the input-output behavior of the crystallizer. However, when looking at the simulated trajectories of the model (see Figure 6), we observe that the dynamics of the

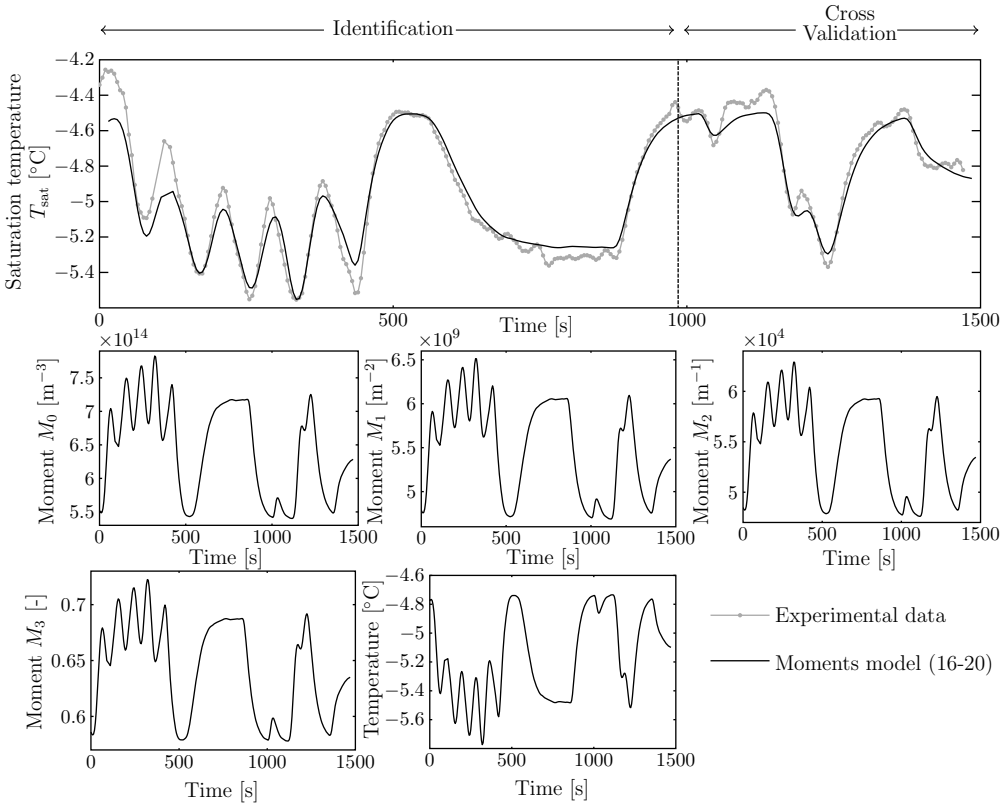

Figure 6: **Parameters identification of the freezer model**: simulated trajectories of the state variables of the identified model, and comparison of the simulated saturation temperature with experimental data (experiment A: $m_{fr} = 50\,kg.h^{-1}$ and $N_{scrap} = 750\,rpm$).

moments M_0, M_1, M_2 and M_3 are close to each other, which suggests that the model could be simplified.

In the control problem point of view, the most important variable of the model is the third moment M_3 on which the variable to be controlled (that is the saturation temperature T_{sat}) depends. The equation of M_3 only depends explicitly on M_3, M_2, T and the inputs m_{fr} and T_e. The link with the other state variables M_0 and M_1 is only made through the variable M_2. As a consequence, if we can find a relation between M_2 and M_3, then we will get a reduced order model only composed of the equations of M_3 and T.

7.1. Mean crystal size and approximation of M_1 and M_2

Assuming crystals of spherical shape, the mean crystal size, denoted L_{mean} in the sequel, can be expressed as the quotient of M_1, that is the sum of crystals lengths, by M_0, that is the total number of crystals:

$$L_{mean} = \frac{M_1}{M_0}. \tag{37}$$

The moment M_3 represents the sum of the volumes of the crystals. By dividing M_3 by L_{mean}, we get a quantity which is representative of the sum of the areas of the crystals. As a consequence, it can be compared to the moment M_2 which also quantify the total area of ice crystals.

Let us first compare the quantities M_2 and $\frac{M_0}{M_1}M_3$ in terms of their dynamic equations. We have:

$$\begin{aligned}\frac{d}{dt}\left(\frac{M_0}{M_1}M_3\right) &= \frac{dM_3}{dt}\frac{M_0}{M_1} + \frac{M_3}{M_1^2}\left(\frac{dM_0}{dt}M_1 - M_0\frac{dM_1}{dt}\right)\\ &= -D\frac{M_0}{M_1}M_3 + G\left(3\frac{M_0}{M_1}M_2 - \frac{M_0^2}{M_1^2}M_3\right)\\ &\quad + N\left(\frac{M_0}{M_1}L_c^3 + \frac{M_3}{M_1} - \frac{M_0M_3}{M_1^2}L_c\right) + B\left(1 - c_1\frac{M_2M_0}{M_1^2}\right)M_3.\end{aligned}$$

Assume now that M_2 is proportional to $\frac{M_0}{M_1}M_3$, and M_1 is proportional to $\frac{M_0}{M_1}M_2$ and denote η_2 and η_1 the proportionality coefficients:

$$M_2 \simeq \eta_2\frac{M_0}{M_1}M_3, \text{ and } M_1 \simeq \eta_1\frac{M_0}{M_1}M_2. \tag{38}$$

We then have $\eta_2\frac{M_0}{M_1}M_2 \simeq \frac{\eta_2}{\eta_1}M_1$ and $\eta_2\frac{M_0^2}{M_1^2}M_3 \simeq \frac{M_0}{M_1}M_2 \simeq \frac{1}{\eta_1}M_1$, so that :

$$3\eta_2\frac{M_0}{M_1}M_2 - \eta_2\frac{M_0^2}{M_1^2}M_3 \simeq \frac{3\eta_2-1}{\eta_1}M_1. \tag{39}$$

In the same way, we get:

$$\eta_2\left(1 - c_1\frac{M_2M_0}{M_1^2}\right) \simeq \frac{\eta_2(\eta_1-c_1)}{\eta_1}, \tag{40}$$

and:

$$\eta_2\left(\frac{M_0}{M_1}L_c^3 + \frac{M_3}{M_1} - \frac{M_0M_3}{M_1^2}L_c\right) \simeq \eta_2\frac{L_c^3}{L_{mean}} + \frac{1}{\eta_1}L_{mean}^2 - \frac{1}{\eta_1}L_{mean}L_c. \tag{41}$$

Let us denote $\tilde{L}_c^2$ the positive quantity $\eta_2\frac{L_c^3}{L_{mean}} + \frac{1}{\eta_1}L_{mean}^2 -$

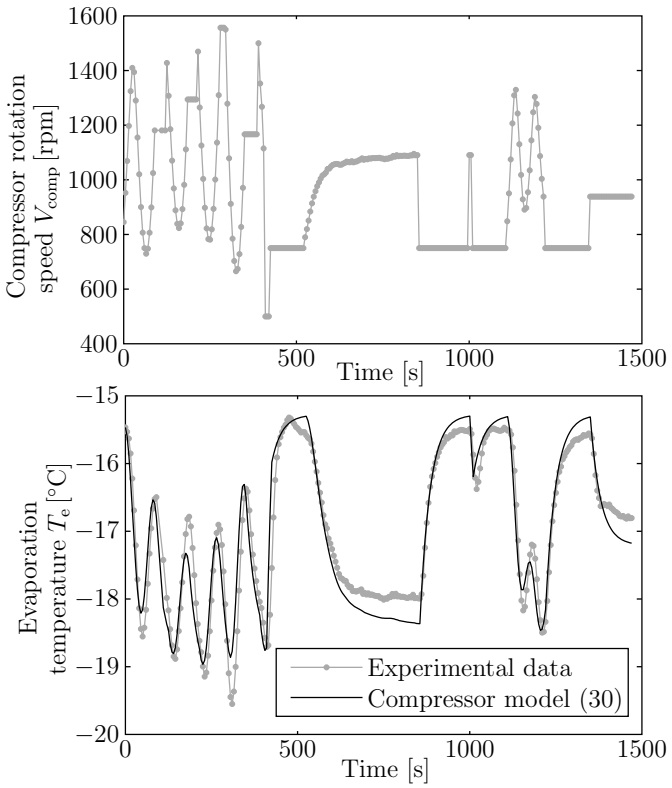

Figure 7: **Model of the compressor - cross validation**. Top: compressor rotation speed V_{comp}. Bottom: evaporation temperature T_e, comparison between experimental data and simulated values. (experiment A: $m_{fr} = 50\,\text{kg.h}^{-1}$ and $N_{\text{scrap}} = 750\,\text{rpm}$)

$\frac{1}{\eta_1} L_{\text{mean}} L_c$.

We finally get:

$$\frac{d}{dt}\left(\eta_2 \frac{M_0}{M_1} M_3\right) \simeq -DM_2 + \frac{3\eta_2 - 1}{\eta_1} GM_1 + N\tilde{L}_c^2 + \frac{\eta_2(\eta_1 - c_1)}{\eta_1} BM_3, \quad (42)$$

$$\text{whereas } \frac{dM_2}{dt} = -DM_2 + \quad 2GM_1 + NL_c^2 + \quad c_2 BM_3. \quad (43)$$

As we can see, both Eqs. (42) and (43) have the same structure. The differences between the two equations can be expressed as variations of the values of the parameters β, ϵ and L_c. Indeed, Eq. (42) can be written exactly with the same expression than Eq. (43), but with:

- $\tilde{\beta} := \frac{3\eta_2 - 1}{2\eta_1}\beta$ in place of β,
- $\tilde{\epsilon} := \frac{\eta_2(\eta_1 - c_1)}{c_2 \eta_1}\epsilon$ in place of ϵ,
- $\tilde{L}_c$ in place of L_c.

According to the sensitivity analysis performed in paragraph 4.1 (see Figure 3), it clearly appears that the parameters β and ϵ do not influence the value of M_2 a lot. As a consequence, if $\tilde{\beta}$ and $\tilde{\epsilon}$ are respectively close to β and ϵ, then the difference between the growth and breakage terms of the two equations will be negligible.

The parameter $\tilde{L}_c$ is not constant because it depends on $L_{\text{mean}} := \frac{M_1}{M_0}$. By simple computations, we can show that, if $1 > \eta_1\eta_2$, the function $L_{\text{mean}} \mapsto \eta_2 \frac{L_c^3}{L_{\text{mean}}} + \frac{1}{\eta_1} L_{\text{mean}}^2 - \frac{1}{\eta_1} L_{\text{mean}} L_c$ is increasing[9] on the interval $[L_c, +\infty)$. Moreover, some experimental studies performed on the process (Arellano et al., 2012) have shown that, in the range of admissible input controls values (see Table 1), and for the same commercial mix than the one considered in this work, the mean crystal size L_{mean} at the outlet of the freezer ranged from $5\mu\text{m} = L_c$ to $9\,\mu\text{m} < 2L_c$.
Under the hypothesis that $L_c < L_{\text{mean}} < 2L_c$, we then conclude that:

$$\eta_2 L_c^2 < \underbrace{\eta_2 \frac{L_c^3}{L_{\text{mean}}} + \frac{1}{\eta_1} L_{\text{mean}}^2 - \frac{1}{\eta_1} L_{\text{mean}} L_c}_{\tilde{L_c}^2} < \frac{\eta_1\eta_2 + 4}{2\eta_1} L_c^2. \quad (44)$$

As a consequence, if $\sqrt{\eta_2}$ and $\sqrt{\frac{\eta_1\eta_2+4}{2\eta_1}}$ are close to 1, then the difference between L_c and $\tilde{L}_c$ will always remain small, which, according to the sensitivity analysis performed in Section 4.1 (see Figure 3), will lead to only small differences between the corresponding values of M_2.

Finally, if $1 > \eta_1\eta_2$, $\frac{3\eta_2-1}{2\eta_1}$, $\frac{\eta_2(\eta_1-c_1)}{c_2\eta_1}$, $\sqrt{\eta_2}$ and $\sqrt{\frac{\eta_1\eta_2+4}{2\eta_1}}$ are close to 1, then the approximation:

$$M_2 \simeq \eta_2 \frac{M_0}{M_1} M_3 \quad (45)$$

can be justified.

Let us check this approximation on some simulations of the model identified from experiment A data (see Figure 6). In Figure 8, are given the plots of $\frac{M_0}{M_1} M_3$ versus M_2, and $\frac{M_0}{M_1} M_2$ versus M_1 of 2 simulations: the one presented in Figure 6 for comparison with the experimental data (simulated data 1), and the simulated response to a random series of steps[10] of V_{comp} (simulated data 2). Both plots exhibit a proportional relationship between the two variables, which, in that case, validates the assumption (38).
The estimated values[11] of η_1 and η_2 are given here after:

$$\eta_1 = 0.8627 \text{ and } \eta_2 = 0.7262, \quad (46)$$

which leads to:

$$\frac{3\eta_2 - 1}{2\eta_1} = 0.6832, \ \frac{\eta_2(\eta_1 - c_1)}{c_2\eta_1} = 0.8916,$$

$$\sqrt{\eta_2} = 0.8522, \text{ and } \sqrt{\frac{\eta_1\eta_2 + 4}{2\eta_1}} = 1.638.$$

For the simulated trajectories presented in Figure 6 (experiment

[9] The derivative of the function is given by $f'(L_{\text{mean}}) = \frac{1}{\eta_1 L_{\text{mean}}^2}\left(-\eta_1\eta_2 L_c^3 + 2L_{\text{mean}}^3 - L_c L_{\text{mean}}^2\right)$ and is such that $f'(L_{\text{mean}}) > 0$, $\forall L_{\text{mean}} \geqslant L_c$, if $1 > \eta_1\eta_2$.

[10] The input V_{comp} is composed of 40 successive steps, the values of which have been randomly chosen in the set $\{200 \times k,\ k = 1 : 13\}$. Each step lasts 300 s, so that the global simulation is 12 000 s long. With such an input, the range of simulated M_3 values is maximal.

[11] These values have been estimated from the simulated response to the V_{comp} steps input (simulated data 2) by use of the least squares method.

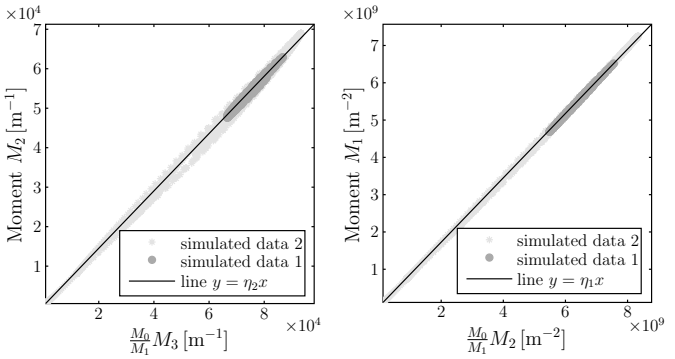

Figure 8: **Approximation of moments M_2 and M_1**: plots of M_2 versus $\frac{M_0}{M_1} M_3$, and M_1 versus $\frac{M_0}{M_1} M_2$. The proportionality coefficients η_1 and η_2 are respectively equal to 0.8627 and 0.7262. (experiment A: $\mathrm{m_{fr}} = 50\,\mathrm{kg.h^{-1}}$ and $N_{\mathrm{scrap}} = 750\,\mathrm{rpm}$)

A), we have:

$$e_{M_1} := \frac{1}{T} \int_{t_0}^{t_0+T} \left| \frac{M_1(t) - \eta_1 \frac{M_0(t)}{M_1(t)} M_2(t)}{M_1(t)} \right| dt = 4.651\,10^{-3},$$

$$e_{M_2} := \frac{1}{T} \int_{t_0}^{t_0+T} \left| \frac{M_2(t) - \eta_2 \frac{M_0(t)}{M_1(t)} M_3(t)}{M_2(t)} \right| dt = 8.690\,10^{-3}.$$

The results obtained with the experiment B are given in Figure 10. For this data set we obtain the following values:

$$\eta_1 = 0.8943,\ \eta_2 = 0.7765,\ e_{M_1} = 7.565\,10^{-3},\ e_{M_2} = 1.876\,10^{-2}. \tag{47}$$

The values of η_1 and η_2 have been computed for each of the 12 experiments. The standard deviation and the minimal, maximal and mean values of η_1 and η_2 (on the set of the 12 experiments) are given in Table 9. We note that the standard deviation is not very large, which means that the values of η_1 and η_2 do not vary a lot from one experiment to the other.

Parameter	Min	Max	Mean	Standard deviation
η_1	0.8529	0.9207	0.8918	0.02101
η_2	0.7077	0.8287	0.7757	0.03692
b_1	$6.001\,10^4$	$1.177\,10^5$	$8.713\,10^4$	$2.069\,10^4$
b_2	$9.911\,10^3$	$4.484\,10^4$	$2.890\,10^4$	$1.113\,10^4$

Table 9: **Identification of parameters for the reduced order model**: identified values of η_1, η_2, b_1 and b_2. The standard deviation and the minimal, maximal and mean values are computed on the set of the 12 experiments.

7.2. Reduced order model

The mean crystal size L_{mean} is a quantity that can be measured (Arellano et al., 2012). If this measurement is available on-line, it can be viewed as an input of the following system composed of only two equations:

$$\frac{dM_3}{dt} = -DM_3 + 3G\frac{\eta_2}{L_{\mathrm{mean}}} M_3 + NL_{\mathrm{c}}^3 \tag{48}$$

$$\frac{dT}{dt} = D(T_0 - T) + K_2(T_{\mathrm{e}} - T) + N_{\mathrm{scrap}}^2 K_3 \mu + K_1 \left(3G\frac{\eta_2}{L_{\mathrm{mean}}} M_3 + NL_{\mathrm{c}}^3 \right). \tag{49}$$

In the case where the measurement of L_{mean} is not available (as it is the case for the data sets considered in this paper), an estimation of L_{mean} has to be considered.
In Arellano et al. (2012), it is shown that when the evaporation temperature decreases, the mean crystal size L_{mean} decreases, whereas the ice mass fraction ϕ_i increases. In other words, the greater the ice mass fraction, the smaller the mean crystal size. As the ice mass fraction ϕ_i is proportional to the moment M_3 (see (12)), we can therefore express L_{mean} as a decreasing function of the moment M_3 (except in the neighborhood of $M_3 = 0$ where the mean crystal size has to be equal to 0). According to the results presented in Arellano et al. (2012), this function does not depend significantly on the dasher rotation speed N_{scrap}, but can vary with the mass flow rate $\mathrm{m_{fr}}$. We so have:

$$L_{\mathrm{mean}} = L_{\mathrm{mean}}(\mathrm{m_{fr}}, M_3), \tag{50}$$

and so, from (45):

$$M_2 \simeq \eta_2 \frac{1}{L_{\mathrm{mean}}(\mathrm{m_{fr}}, M_3)} M_3 := M_2(\mathrm{m_{fr}}, M_3), \tag{51}$$

where $M_3 \mapsto M_2(\mathrm{m_{fr}}, M_3)$ is a positive function which is increasing when $M_3 \mapsto L_{\mathrm{mean}}(\mathrm{m_{fr}}, M_3)$ is decreasing[12]. This finally leads to the following reduced order model:

$$\frac{dM_3}{dt} = -DM_3 + 3GM_2(\mathrm{m_{fr}}, M_3) + NL_{\mathrm{c}}^3 \tag{52}$$

$$\frac{dT}{dt} = D(T_0 - T) + K_2(T_{\mathrm{e}} - T) + N_{\mathrm{scrap}}^2 K_3 \mu + K_1 \left(3GM_2(\mathrm{m_{fr}}, M_3) + NL_{\mathrm{c}}^3 \right). \tag{53}$$

The determination of the expression of $L_{\mathrm{mean}}(\mathrm{m_{fr}}, M_3)$ can be made from experimental measurements of the mean crystal size, as the ones presented in Arellano et al. (2012). However, in our case, recall that the objective is to get a model which accurately describes the time evolution of the saturation temperature, in an input-output point of view. As a consequence, the identification of $L_{\mathrm{mean}}(\mathrm{m_{fr}}, M_3)$ (and of $M_2(\mathrm{m_{fr}}, M_3)$) will be made directly from the numerical simulations.

Consider the model identified from experiment A data (Figure 6), for which $\mathrm{m_{fr}} = 50\,\mathrm{kg.h^{-1}}$. The plots of M_2 versus M_3, and $\frac{M_1}{M_0}$ (= L_{mean}) versus M_3 are given in Figure 9 for the simulated data 1 (simulated trajectories of experiment A) and 2 (simulated response to the V_{comp} steps input). The plot of M_2 versus M_3 shows a relationship between the two variables

[12] The derivative of function $f : M_3 \mapsto M_2(\mathrm{m_{fr}}, M_3)$ is given by $f'(M_3) = \frac{1}{L_{\mathrm{mean}}(\mathrm{m_{fr}}, M_3)^2} \left(\eta_2 L_{\mathrm{mean}}(\mathrm{m_{fr}}, M_3) - \eta_2 \partial_{M_3} [L_{\mathrm{mean}}(\mathrm{m_{fr}}, M_3)] M_3 \right)$.

close to a line. However, to be physically realistic, the function $M_3 \mapsto M_2(\mathrm{m_{fr}}, M_3)$ has to be such that $M_2(\mathrm{m_{fr}}, 0) = 0$. As a consequence, we have considered a function of the form:

$$M_2(\mathrm{m_{fr}}, M_3) = M_3^{\lambda} \left[b_1(\mathrm{m_{fr}}) M_3 + b_2(\mathrm{m_{fr}}) \right], \ \lambda > 0. \qquad (54)$$

To obtain a good estimation of L_{mean}, we also need to have $L_{\mathrm{mean}}(\mathrm{m_{fr}}, 0) = 0$ (see the plot of $\frac{M_1}{M_0}$ versus M_3), which leads to the constraint $\lambda < 1$ (because from (51), $L_{\mathrm{mean}}(\mathrm{m_{fr}}, M_3) = \eta_2 M_3^{1-\lambda} / \left[b_1(\mathrm{m_{fr}}) M_3 + b_2(\mathrm{m_{fr}}) \right]$). Several values of λ have been tested. The functions identified with the least squares method from the simulated data 2 are plotted in Figure 9. The identified functions $M_3 \mapsto L_{\mathrm{mean}}(50, M_3)$ and $M_3 \mapsto M_2(50, M_3)$ obtained with $\lambda = 3/4$ are the ones which fit the simulated data at best. The corresponding identified values of $b_1(50)$ and $b_2(50)$ are given here after :

$$b_1(50) = 6.001\, 10^4,\ b_2(50) = 3.731\, 10^4. \qquad (55)$$

Some experimental data taken from the paper of Arellano

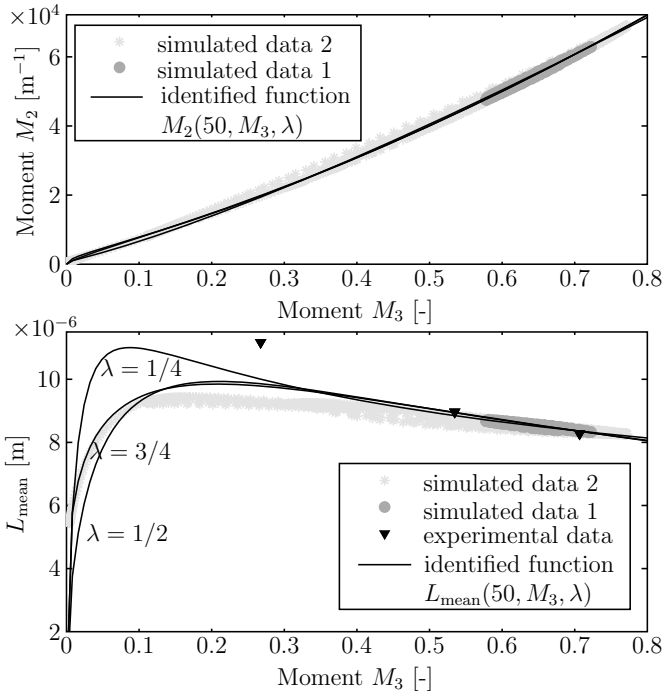

Figure 9: **Reduced order model**: plots of M_2 versus M_3, and $M_1/M_0 (= L_{\mathrm{mean}})$ versus M_3 for identification of the functions $M_3 \mapsto M_2(\mathrm{m_{fr}}, M_3)$ and $M_3 \mapsto L_{\mathrm{mean}}(\mathrm{m_{fr}}, M_3)$. (experiment A: $\mathrm{m_{fr}} = 50\,\mathrm{kg.h^{-1}}$ and $N_{\mathrm{scrap}} = 750\,\mathrm{rpm}$)

et al. (2012) have also been considered for comparison with the identification function $L_{\mathrm{mean}}(50, M_3)$. Among the 15 experiments presented in Arellano et al. (2012), 3 have been performed[13] with the same values of the mass flow rate and the dasher rotation speed than the ones used for the numerical simulation of Figure 9, that is $\mathrm{m_{fr}} = 50\,\mathrm{kg.h^{-1}}$ and $N_{\mathrm{scrap}} = 750\,\mathrm{rpm}$. The 3 experiments are presented in Table 10 in which the evaporation temperature, and the mean values of both the ice mass fraction and the mean chord length are given. The 3 experimental data points represented in Figure 9 correspond to these 3 experiments. The plotted values have been deduced from the values given in Table 10 in the following way:

T_{e} [°C]	mean chord length [μm]	ϕ_i [%]
-15.3 ± 0.1	6.5 ± 0.2	28
-19.8 ± 0.1	6 ± 0.2	37
-10.6 ± 0.1	8.1 ± 0.1	14

Table 10: **Experimental data from the paper Arellano et al. (2012)**: evaporation temperature, mean chord length and ice fraction values measured during a crystallization performed with $\mathrm{m_{fr}} = 50\mathrm{kg.h^{-1}}$ and $N_{\mathrm{scrap}} = 750\,\mathrm{rpm}$.

- the value of M_3 is deduced from ϕ_i by the relation (12).
- the value of L_{mean} is not directly equal to the Mean Chord Length (MCL). Indeed, as explained in Wynn (2003), the MCL of a sphere is $\pi/4 \simeq 0.785$ times smaller than its diameter. This value is nevertheless theoretical; the values of L_{mean} in Figure 9 are obtained by dividing the MCL by 0.725.

The identified function $L_{\mathrm{mean}}(50, M_3)$, and the quantity $\frac{M_1}{M_0}$, give a good estimation of the mean crystal size for the largest values of M_3. For small values of M_3, the estimation is less good, but the qualitative behavior remains consistent.

The values of $b_1(\mathrm{m_{fr}})$ and $b_2(\mathrm{m_{fr}})$ have been computed for each of the 12 experiments considered in this paper. The standard deviation and the minimal, maximal and mean values of $b_1(\mathrm{m_{fr}})$ and $b_2(\mathrm{m_{fr}})$ (on the set of the 12 experiments) are given in Table 9. For all the 12 experiments, the approximation (54) with $\lambda = 3/4$ leads to a good input-output approximation of the system. The results obtained with the experiment B are given in Figure 10. For this data set, we get the following identified values:

$$b_1(25) = 1.070\, 10^5,\ b_2(25) = 9.911\, 10^3. \qquad (56)$$

8. Comparison between the reduced order model (52-54) and the moments model (16-20)

To validate the reduced order model (52-54), the steady states values of the model are first compared with the ones of the moments model (16-20). Unfortunately, due to the complexity of these models and because it depends on the expressions of T_{sat} and μ, neither the values nor the number of equilibrium points can be analytically computed. However, these quantities can be computed numerically for some given values of the model parameters and several set of admissible physical values of the input variables (see Casenave et al. (2012) for a steady-states analysis of the moments model (16-20)).

In Figure 11, the computed steady-states values of both models (52-54) and (16-20) are given for different values of the evaporation temperature T_{e} and the dasher rotation speed N_{scrap}. For the computation, the set of model parameters is the one used for experiment B (see Figure 10). The mass flow rate is equal to $25\,\mathrm{kg.h^{-1}}$ and the function $M_3 \mapsto M_2(25, M_3)$ is assumed to

[13] The 3 experiments we are talking about are the runs number 10, 13 and 14 of Table 1 in Arellano et al. (2012).

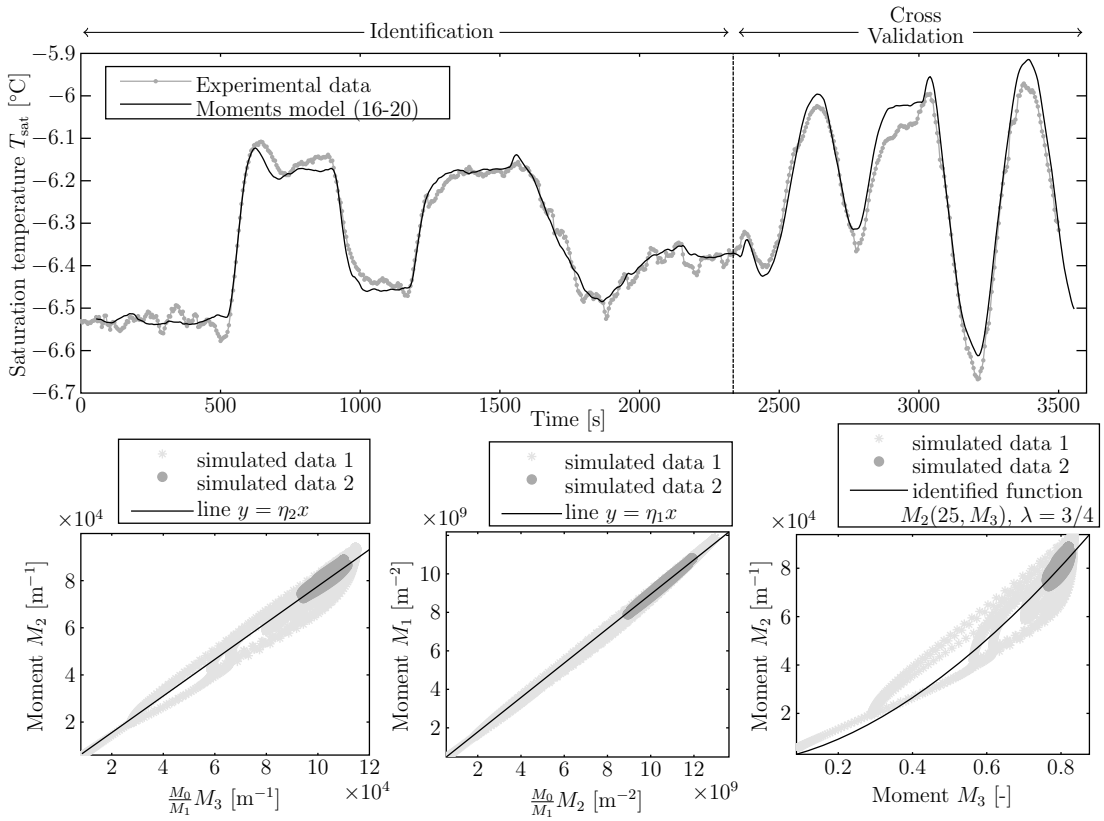

Figure 10: **Parameters identification of the freezer model**: Top: simulated trajectories of the saturation temperature and comparison with experimental data. Bottom: plots of M_2 versus $\frac{M_0}{M_1} M_3$, M_1 versus $\frac{M_0}{M_1} M_2$, and M_2 versus M_3. (experiment B: m_{fr} = 25 kg.h^{-1} and N_{scrap} = 750 rpm).

be of the form (54) with the values of $b_1(25)$ and $b_2(25)$ given in (56) and with $\lambda = 3/4$. As we can see, the steady-states values of the two models are really close to each other, which is a first validation of the reduced order model. Similar results are obtained for other values of the mass flow rate m_{fr}.

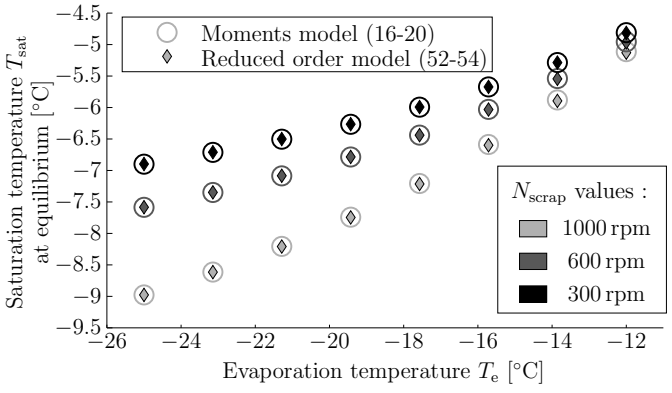

Figure 11: **Steady states comparison between the reduced order model (52-54) and the moments model (16-20)**. (experiment B: m_{fr} = 25 kg.h^{-1})

To go further in the validation of the reduced order model, we also have compared the trajectory of the saturation temperature T_{sat} obtained by the simulation of model (52-54) with the one obtained by the simulation of the moments model (16-20). Consider the data set of experiment A (see Figure 6). In that case, the trajectories obtained by simulation of both models are so close to each other that we cannot distinguish them when they are plotted on the same figure. We indeed have :

$$\frac{1}{T}\int_{t_0}^{t_0+T} \left| \frac{T_{sat}^{(16-20)}(t) - T_{sat}^{(52-54)}(t)}{T_{sat}^{(16-20)}(t)} \right| dt = 6.850\,10^{-5}, \qquad (57)$$

where $T_{sat}^{(16-20)}$ (respectively $T_{sat}^{(52-54)}$) is the trajectory obtained by the simulation of model (16-20) (respectively model (52-54)). For the experiment B (see Figure 10), this quantity is equal to $8.587\,10^{-5}$.

9. Conclusion

The present paper focuses on the identification and the reduction of a model of an ice cream crystallization process. The model which is initially considered is a dynamic version of the one presented in Arellano et al. (2013) and Gonzalez et al. (2011). It is composed of 5 ordinary differential equations which describe the dynamics of the 4 first moments of the CSD and of the ice temperature. The first part of the paper consists in the identification of the model parameters whereas the second part focuses on the model reduction. It is shown that, to accurately describe the input-output behavior of the system (the input and output variables being respectively the evaporation temperature and the saturation temperature) whatever the

conditions are, it is sufficient to consider a reduced order model composed of 2 ODEs (one for the third moment M_3 and one for the ice temperature T) and to modify the values of only two model parameters: the convective heat transfer coefficient h_e, and the viscous dissipation coefficient χ. In a control point of view, it has a real interest: adaptive control techniques can indeed be used to modify the values of h_e and χ in such a way that the process is controlled in all conditions.
Coupling with a black box model (first order equation with a nonlinear gain) for the modeling of the compressor, the reduced order model of the crystallization process is finally written:

$$\begin{aligned}\frac{dM_3}{dt} &= -DM_3 + 3GM_2 + NL_c^3\\ \frac{dT}{dt} &= D(T_0 - T) + K_2(T_e - T) + N_{scrap}^2 K_3 \mu + K_1\left(3GM_2 + NL_c^3\right)\\ \frac{dT_e}{dt} &= -\frac{1}{\tau_c}T_e + \frac{1}{\tau_c}G^c(V_{comp}, m_{fr}),\end{aligned}$$

with $\mu = \mu(M_3, T, N_{scrap}, \chi)$, $G = G(M_3, T)$, $N = N(M_3, T_e)$, $K_2 = K_2(h_e)$, $K_3 = K_3(\chi)$ and $M_2 = M_2(m_{fr}, M_3) = M_3^{\lambda}\left[b_1(m_{fr})M_3 + b_2(m_{fr})\right]$.

The problem of the control of the ice cream viscosity will be studied in a further paper, on the basis of this model.

References

Arellano, M., Benkhelifa, H., Alvarez, G., Flick, D., 2013. Coupling population balance and residence time distribution for the ice crystallization modeling in a scraped surface heat exchanger. Chemical Engineering Science 102, 502–513.

Arellano, M., Benkhelifa, H., Flick, D., Alvarez, G., 2012. Online ice crystal size measurements during sorbet freezing by means of the focused beam reflectance measurement (FBRM) technology. Influence of operating conditions. Journal of Food Engineering 113, 351–359.

Bernard, O., Hadj-Sadok, Z., Dochain, D., Genovesi, A., Steyer, J.P., 2001. Dynamical model development and parameter identification for an anaerobic wastewater treatment process. Biotechnology and bioengineering 75, 424–438.

Casenave, C., Dochain, D., Alvarez, G., Benkhelifa, H., Flick, D., Leducq, D., 2012. Steady-state and stability analysis of a population balance based nonlinear ice cream crystallization model, in: American Control Conference (ACC), IEEE, june 27-29 2012, Montréal (Canada). pp. 6461–6466.

Christofides, P., 2002. Nonlinear model reduction and control of particulate processes, in: Particle Technology Series: Model-Based Control of Particulate Processes. Kluwer Academic Publishers, Dordrecht (The Nederlands). volume 14, pp. 9–33.

Christofides, P., El-Farra, N., Li, M., Mhaskar, P., 2008. Model-based control of particulate processes. Chemical Engineering Science 63, 1156–1172.

Cook, K., Hartel, R., 2010. Mechanisms of Ice Crystallization in Ice Cream Production. Comprehensive Reviews in Food Science and Food Safety 9, 213–222.

Costa, C., Maciel, M., Filho, R., 2007. Considerations on the crystallization modeling: Population balance solution. Computers & Chemical Engineering 31, 206–218.

Dokucu, M.T., Park, M.J., Doyle III, F.J., 2008. Reduced-order methodologies for feedback control of particle size distribution in semi-batch emulsion copolymerization. Chemical Engineering Science 63, 1230–1245.

Garnier, H., Young, P., 2004. Time-domain approaches to continuous-time model identification of dynamical systems from sampled data, in: American Control Conference, June 30 - July 2 2004, Barcelona, Spain. pp. 667–672.

Gonzalez, J.E., 2012. Contribution au contrôle par la modélisation d'un procédé de cristallisation en continu. Ph.D. thesis. Agroparistech.

Gonzalez, J.E., Arellano, M., Leducq, D., Alvarez, G., Benkhelifa, H., Flick, D., 2011. Moments model for a continuous sorbet crystallization process, in: The 23rd IIR International Congress of Refrigeration. August 21-26 2011, Prague, Czech Republic.

Hartel, R.W., 2001. Crystallization in foods. Aspen Publishers Gaithersburg.

Ma, C.Y., Wang, X.Z., 2012. Closed-loop control of crystal shape in cooling crystallization of l-glutamic acid. Journal of Process Control 22, 72–81.

Mantzaris, N.V., Daoutidis, P., 2004. Cell population balance modeling and control in continuous bioreactors. Journal of Process Control 14, 775–784.

Mesbah, A., Nagy, Z.K., Huesman, A.E.M., Kramer, H.J.M., Van den Hof, P.M.J., 2012. Nonlinear model-based control of a semi-industrial batch crystallizer using a population balance modeling framework. Control Systems Technology, IEEE Transactions on 20, 1188–1201.

Motz, S., Mannal, S., Gilles, E.D., 2004. Integral approximation - an approach to reduced models for particulate processes. Chemical Engineering Science 59, 987–1000.

Mullin, J., 2001. Crystallization. Butterworth-Heinemann, Woburn (Massachusetts, USA).

Nagy, Z.K., 2008. A population balance model approach for crystallization product engineering via distribution shaping control. Computer Aided Chemical Engineering 25, 139–144.

Nagy, Z.K., Chew, J.W., Fujiwara, M., Braatz, R.D., 2008. Comparative performance of concentration and temperature controlled batch crystallizations. Journal of Process Control 18, 399–407.

Randolph, A., 1971. Theory of particulate processes: analysis and techniques of continuous crystallization. Academic press, New York (USA).

Rawlings, J., Miller, S., Witkowski, W., 1993. Model identification and control of solution crystallization processes: a review. Industrial & Engineering Chemistry Research 32, 1275–1296.

Ray, W., 1978. Some recent applications of distributed parameter systems theory - A Survey. Automatica 14, 281–287.

Sheikhzadeh, M., Trifkovic, M., Rohani, S., 2008. Real-time optimal control of an anti-solvent isothermal semi-batch crystallization process. Chemical Engineering Science 63, 829–839.

Vollmer, U., Raisch, J., 2006. Control of batch crystallization - A system inversion approach. Chemical Engineering and Processing: Process Intensification 45, 874–885.

Wynn, E., 2003. Relationship between particle-size and chord-length distributions in focused beam reflectance measurement: stability of direct inversion and weighting. Powder Technology 133, 125–133.

Young, P.C., 2002. Optimal IV identification and estimation of continuous-time TF models, in: 15th Triennial IFAC world congress on automatic control, July 21-26 2002, Barcelona, Spain.